Title
Effect of salt concentration profiles on protrusion growth in lithium-polymer-lithium cells

Authors
Frenck, Louise
Veeraraghavan, Vijay D
Maslyn, Jacqueline A
et al.

Publication Date
2020-12-01

DOI
10.1016/j.ssi.2020.115517

Peer reviewed

Effect of Salt Concentration Profiles on Protrusion Growth in Lithium-polymer-lithium Cells

Louise Frenck[a,b], Vijay D. Veeraraghavan[a], Jacqueline A. Maslyn[a,b], Alexander Müller[c,d], Alec S. Ho[a,b], Whitney. S. Loo[a], Andrew M. Minor[c,d], Nitash P. Balsara[a,b]

[a]Department of Chemical and Biomolecular Engineering, University of California, Berkeley, California 94720, United States

[b]Materials Sciences Division, Lawrence Berkeley National Laboratory, Berkeley, California 94720, United States

[c]National Center for Electron Microscopy, Molecular Foundry, Lawrence Berkeley National Laboratory, Berkeley, California 94720, United States

[d]Department of Materials Science and Engineering, University of California, Berkeley, California 94720, United States

KEYWORDS: “Lithium”, “Polymer Electrolyte”, “Salt Concentration”, “Rechargeable Batteries”, “Salt Concentration Gradient”, “Concentrated Solution Theory”, “Electrochemical Properties”.

ABSTRACT

The formation of dendrites and other protrusions on lithium metal anodes is a subject of continued interest due to the potential to incorporate these anodes in next-generation rechargeable batteries with increased energy densities. Solid polymer electrolytes show improved stability against lithium metal compared to liquid carbonate electrolytes. We have studied the effect of salt concentration on the formation of protrusions formed on electrodeposited lithium through a rigid block copolymer electrolyte, polystyrene-*block*-poly(ethylene oxide) (PS-*b*-PEO or SEO), in a lithium-lithium symmetric cell. The cell lifetime decreases by a factor of 100 when salt concentration is increased by a factor of 5. Our main objective is to understand the reason for this observation. We show that this decrease is not due to a salt-induced change of the morphology of the block-copolymer electrolyte, nor is it due to a salt-induced change of mechanical properties. We use an approach based on Newman's concentrated solution theory to fully characterize ion transport in the block-copolymer electrolyte, and report the conductivity, salt diffusion coefficient, cation transference number, and thermodynamic factor. Neither cell lifetime nor protrusion density in failed cells correlate with any of these electrochemical parameters. However, the electrochemical parameters can be used to predict salt concentration profiles in our symmetric cells. We posit that an important parameter in protrusion growth is the magnitude of the salt concentration gradient, Δ. We observe a direct correlation between Δ and lithium protrusion growth.

INTRODUCTION

The formation of dendrites and other protrusions on lithium metal anodes[1–5] is a subject of continued interest due to the potential to incorporate them in rechargeable batteries with high energy densities.[6–10] Numerous theoretical and experimental studies aim to determine the underpinnings of dendrite growth on lithium metal anodes.[11–16] Several studies on solid polymer electrolytes show improved chemical stability and cycling reversibility against lithium metal.[17–23] In practical batteries, electrolytes with higher salt concentrations are necessary to maximize the flux of lithium ions.[24–26]

The work presented here builds on previous studies in which we investigated the effect of temperature[27], current density,[28] and salt concentration[29] on the electrodeposition of lithium through block copolymer electrolytes. In a previous study[29], we uncovered the effect of salt concentration on the formation of protrusions formed on electrodeposited lithium through a rigid block copolymer electrolyte, polystyrene-*block*-poly(ethylene oxide) (PS-*b*-PEO or SEO) mixed with LiTFSI (lithium bis(trifluoromethanesulfonyl) imide). Li/SEO/Li symmetric cells were cycled at a fixed current density and the cycle life was found to decrease rapidly with increasing salt concentration. The purpose of this work is to determine the reason for this decrease in cycle life. In particular, we show that this decrease is not due to a salt-induced change of the morphology of the block-copolymer electrolyte, nor is it due to a salt-induced change of mechanical properties. We use the Newman approach[30] to characterize the block-copolymer electrolyte, and report the conductivity, salt diffusion coefficient, cation transference number and thermodynamic factor. These parameters are used to predict salt concentration profiles in our

symmetric cells.[31] We find a strong correlation between the nature of these concentration profiles and cell lifetime.

METHODS

Materials. In this study, we used a polystyrene-*block*-poly(ethylene oxide) copolymer electrolyte (SEO), which was synthesized by anionic polymerization, as described in previous work.[32–34] The molar masses of the PS and PEO blocks were 235 and 222 kg mol^{-1}, respectively, with a PEO volume fraction of 0.475 without salt and an overall polydispersity index of 1.05. Methods for electrolyte preparation and electrochemical cycling mimicked those previously reported by Maslyn *et al.[28,35–37]* All electrolyte preparation and lithium cell assembly steps were performed in an argon filled glovebox with less than 1 ppm of water and less than 1 ppm of oxygen to avoid any contamination.

Electrolyte preparation. Methods for electrolyte preparation and electrochemical cell fabrication closely mimicked those previously reported.[29] The salt used in this study was lithium bis(trifluoromethanesulfonyl) imide (LiTFSI). The average salt concentration, r_{av}, defined as the molar ratio of lithium cations to the ether oxygen, varied from 0.04 to 0.20. For simplicity, we in the following refer to the set of electrolytes as SEO electrolyte.

Ionic conductivity. Ionic conductivity measurements were performed using both aluminum/SEO/aluminum symmetric cells and Li/SEO/Li symmetric cells. Cells were assembled

using punched SEO electrolyte membranes with a diameter of 3/8 inch and two aluminum blocking electrodes or lithium metal non-blocking electrodes (FMC), backed with nickel foil, of 5/16 inch diameter. The obtained aluminum sandwiches were pressed in a hand-press at 90 ºC for 10 s, while the obtained lithium sandwiches were pressed in a hand-press at room temperature for 10 s. Then, aluminum tabs were added and assembled cells were vacuum sealed inside a laminated aluminum pouch material (Showa-Denko) in order to carry out experiments outside of the glovebox. Cells were placed in a custom heating stage. First, cells were annealed at 120 ºC for 4 h in order to ensure good contact and erase the electrolyte's temperature history. Next, the cells were decreased to room temperature and then heated up to 90 ºC and equilibrated for 1 h prior to the electrochemical measurements. Ionic conductivity measurements were measured by ac impedance spectroscopy using a BioLogic VMP3 potentiostat. Complex electrochemical impedance spectra were acquired for a frequency range from 1 MHz to 1 Hz at an amplitude of 10 mV. The data were analyzed in the form of a Nyquist plot and an electrical equivalent circuit was used to fit the data and obtain the bulk resistance to calculate the ionic conductivity.

Current fraction and restricted diffusion experiments. Steady-state current fraction and restricted diffusion measurements were performed using Li/SEO/Li symmetric cells (same assembly method as lithium metal ionic conductivity cells) and a BioLogic VMP3 potentiostat. All measurements were performed at 90°C. To ensure stable interfacial layers at the lithium-polymer interfaces, 15 charge (positive current density applied)/discharge (negative current density applied) conditioning cycles at a low current density of 0.02 mA cm^{-2} were performed prior to the measurements. Each conditioning cycle consisted of a 4 h charge followed by a 45

5

min rest and a 4 h discharge. Ac electrochemical impedance spectroscopy was performed before polarization. Impedance spectra were measured from 1 MHz to 1 Hz at an amplitude of 10 mV. The data were plotted in the form of Nyquist plots and analyzed using equivalent electrical circuits. The steady-state current fraction experiment consisted of applying a potential of ΔV = 10 mV and measuring the current at time intervals of 2 s for 2 h, a time long enough to reach steady-state current. Ac impedance spectra were measured every 20 min.

In the absence of a concentration gradient (i.e. prior to polarization), the calculated initial current, i_{Ω}, is defined by the Ohm's law as given in Equation 1, where ΔV is the potential applied, and $R_{i,0}$ and $R_{b,0}$ the initial resistances measured for the interface and the bulk respectively.

$$i_{\Omega} = \frac{\Delta V}{R_{i,0} + R_{b,0}} \qquad \textit{Equation 1}$$

The current fraction, $\rho_{+¿¿}$, was calculated according to Equation 2, where $R_{i,SS}$ is the resistance of the interface at steady-state, and i_{SS} is the steady-state current.[38,39]

$$\rho_{+¿} = \frac{i_{SS}(\Delta V - i_{\Omega} R_{i,0})}{i_{\Omega}(\Delta V - i_{SS} R_{i,SS})}¿ \qquad \textit{Equation 2}$$

The restricted salt diffusion coefficients were measured using the polarization induced by the current fraction experiment. The potential applied was stopped and cells were allowed to relax for 4 h while the open-circuit voltage, *U*, was recorded at time interval of 1 s. The restricted salt diffusion coefficient, D, was calculated according to:

$$\frac{-d\ln U}{dt} = \frac{\pi^2 D}{L}, \qquad \textit{Equation 3}$$

where L is the thickness of the electrolyte, and the left side of Equation 3 is the slope from the least-squares fit of –ln U vs. time.

Galvanostatic experiments. Methods to prepare, condition and cycle Li/SEO/Li symmetric cells can be found in previous work by Frenck *et al*.[29]

Scanning Electron Microscopy. Three samples were prepared for morphology analysis. The SEO block-copolymer was dissolved in N-methylpyrrolidone, (NMP), and mixed with LiTFSI salt such that r_{av} was equal to 0.04, 0.085 and 0.12. .Then each solution was drop casted on a silicon wafer. The solvent was evaporated at 60 ºC on a casting plate, and then the samples were dried at 90 ºC under active vacuum for 3 days prior to the experiment. Samples were transferred to the SEM facility using an air-tight desiccator. To prevent charging artefacts, a Gatan Sputter Coater was used to coat all samples with an approximately 2 nm thick carbon layer. The morphology of the samples was investigated using a FEI Helios G4 UX scanning electron microscope operated at 2 kV. Secondary electron images were acquired using the through-lens detector.

Linear Rheology experiments. All sample preparation was performed inside an argon filled glove box. Three samples were prepared: one neat polymer sample, and two SEO electrolytes with r_{av} = 0.085 and r_{av} = 0.20, respectively. The neat SEO sample was prepared by adding polymer into a 1 mm thick polycarbonate spacer with a 9 mm diameter hole, and pressing it between two Teflon sheets in a hand press heated to 120 ºC. The sample was pressed at this temperature for 4 h and then removed from the spacer using a metal punch. The two salt-containing samples were prepared by first casting polymer electrolyte membranes (see electrolyte preparation). Then the membrane was punched to obtain 9 mm disks, which were hot

pressed together inside a hand press at 110 ºC until a 1 mm thick disk was obtained. After preparation, the final samples were transferred in a desiccator to a Rheometric Scientific ARES Rheostat. Prior to the experiment, the rheometer plattens were cleaned and heated up to 90 ºC under a flow of dry nitrogen. In addition, the gap between the plattens was zeroed. The samples were then placed between the plattens; samples were in contact with air for less than 30 s before the nitrogen-purged oven was closed.

Samples were first annealed at 120 ºC for 1 h. Then, the temperature was decreased to 90 ºC, the temperature used for measurements. Samples were left to equilibrate for 1 h at 90 ºC prior to the measurement. First, a dynamic strain sweep test was performed at a frequency of 1 rad s^{-1} to ensure measurement in the linear regime between stress and strain. Then a frequency sweep test was performed from 1 to 100 rad s^{-1} at the chosen strain. In order to ensure good adhesion between the plattens and the sample, a normal force between 10 and 40 gm was applied during measurement. One sample of each polymer type was made due to limited material; however, measurements were repeated 3 times and averaged.

RESULTS AND DISCUSSION

Figure 1 summarizes results of cell cycling experiments on Li/SEO/Li symmetric cells as a function of average salt concentration in the SEO electrolyte. These results are taken from reference [29]. In each cycle, a steady current density of 0.175 mA cm^{-2} was applied for 4 hours in one direction followed by 45 minutes of rest and another 4 hours of the same steady current in the opposite direction followed by 45 minutes of rest. The average number of cycles to failure is plotted as a function of r_{av} in Figure 1. The right ordinate converts cycles to charge density passed before failure, including charge passed during the conditioning cycles (8.64 C cm^{-2}). Cells

fail due to short circuit when a growing protrusion from one electrode touches the opposite electrode. The cell lifetime decreases rapidly with average salt concentration between r_{av} = 0.04 and r_{av} = 0.15. The cell lifetime at r_{av} = 0.04 is a factor of 10 larger than that at r_{av} = 0.15. Between r_{av} = 0.15 and r_{av} = 0.20 the cell lifetime remains low but increases slightly. Our main objective is to understand the reason for the large decrease in cell lifetime presented in Figure 1. We present our understanding based on three sets of characterization results: electron microscopy, rheology and electrochemical characterization.

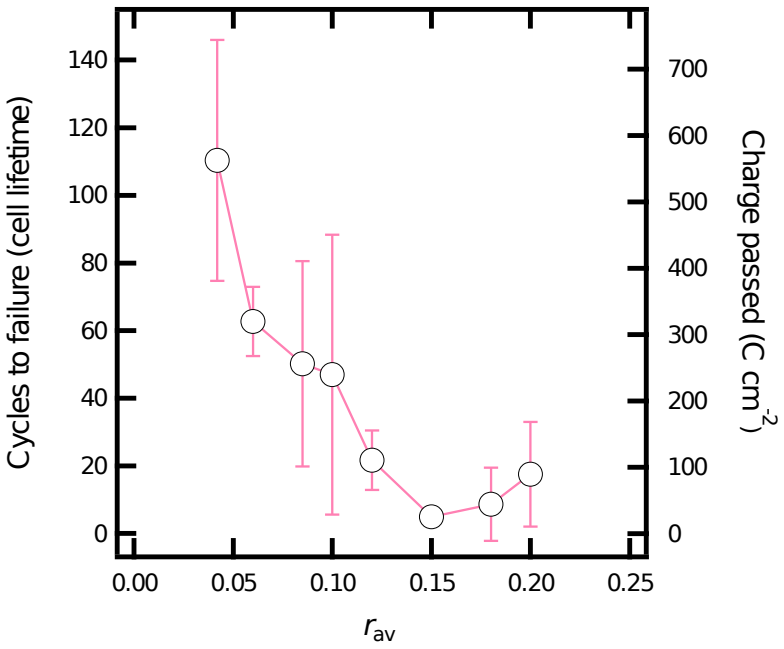

Figure 1. Average number of cycles to failure (cell lifetime) at 90 ^{o}C (left *y* axis) as a function of salt concentration in the SEO electrolyte, r_{av}. The cycles shown do not include the conditioning cycles. Charge density passed just before failure, C_d, is shown on the right *y* axis, where charge density passed during conditioning is included (8.64 C cm^{-2}). Error bars represent the standard deviation from 3 to 6 cells. Data taken from reference [29].

9

The morphologies of three electrolytes at r_{av} = 0.04, r_{av} = 0.085, and r_{av} = 0.12 are shown in Figure 2. All electron micrographs show lamellae, with bright PEO lamellae alternating with dark PS lamellae. This morphology is consistent with the volume fraction of the PEO-rich microphase in our electrolytes.[40,41] The micrographs in Figure 2 were obtained at room temperature and do not necessarily represent the grain structures in the symmetric cells at 90 ^{o}C. We suspect that the formation of spherulites (defined as radial centrosymmetric organization of crystals often seen in semi-crystalline polymers) at r_{av} = 0.04 is due to effects related to the crystallization of the PEO block. Differential scanning calorimetry experiments (DSC) indicate that the sample at r_{av} = 0.04 is crystalline at room temperature with a melting point at 57 ^{o}C and a crystallinity percentage of 45%, while r_{av} = 0.085 presents a melting temperature at 43 ^{o}C with a low crystallinity percentage of 2%, and r_{av} = 0.12 is completely amorphous at room temperature (see DSC data and methods in supplemental information Figure S1). Our cycling and electrochemical data were obtained at 90 ^{o}C, where all of the electrolytes are amorphous. We expect the morphology of the r_{av} = 0.04 electrolyte at 90 ^{o}C to be similar to that shown in Figures 2(b) and (c). The glass transition temperature, T_g, of the PS phase is roughly 108 ^{o}C for the whole range of salt concentrations (see Figure S2 in SI). The domain spacing of the lamellae phases (center to center distance between adjacent PS lamellae) is not a strong function of salt concentration and is, on average, 165 nm, in the micrographs in Figure 2. This value is consistent with previous reports.[42] The SEM data in Figure 2 show that the decrease in cell lifetime by a factor of 5 when r_{av} increases from 0.04 to 0.12 cannot be attributed to a change in electrolyte morphology.

10

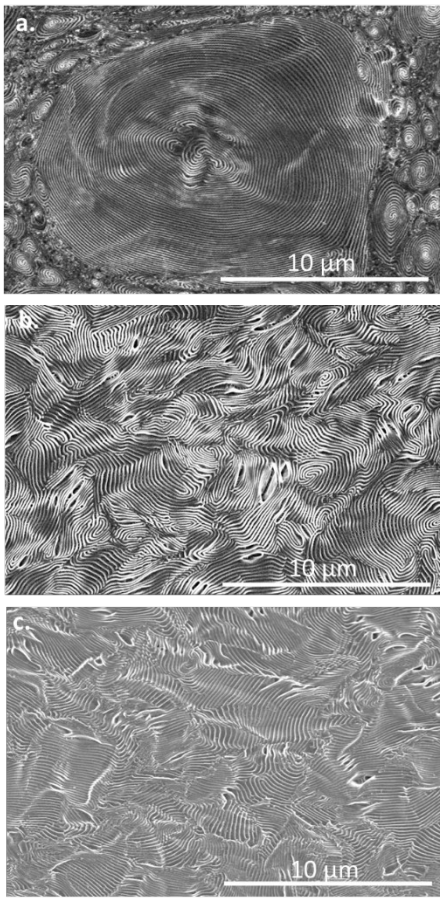

Figure 2. Electron micrographs of SEO electrolytes at room temperature. (a) r_{av} = 0.04, (b) r_{av} = 0.085 and (c) r_{av} = 0.12. The morphology of the r_{av} = 0.04 sample is distorted due to crystallization of the PEO block. All of the ion transport experiments were conducted in the amorphous state pictured in (b) and (c). We expect the morphology of the r_{av} = 0.04 sample in the amorphous state to be similar to Figures (b) and (c).

The relationship between mechanical properties of the electrolyte and cycle life of Li/SEO/Li symmetric cells has been discussed extensively in the literature,[27,37,43] starting with pioneering work by Monroe and Newman.[24,44,45]

Figure 3 shows the frequency dependency of storage (*G'*) and loss (*G"*) shear moduli of SEO, measured at 90 ^{o}C, as a function of increasing average salt concentration (from neat to r_{av}

11

= 0.20). All three samples are viscoelastic solids where in *G'* is significantly larger than *G"*. In theory, the growth of protrusion through electrolytes is a slow process governed by the low frequency shear modulus. The data in Figure 3 indicate no deterioration in the low frequency shear modulus in SEO electrolytes as a function of increasing average salt concentration. Thus, it is evident that the rapid decrease in cycle life seen in Figure 1 is not related to mechanical properties.

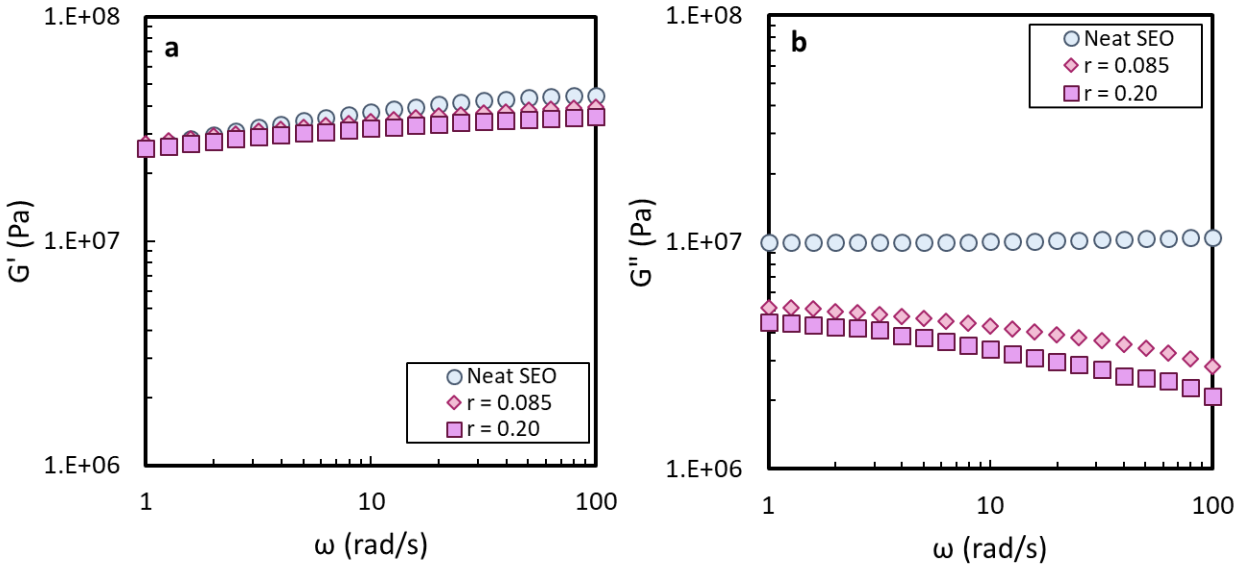

Figure 3. Frequency (ω) dependence of (a) storage (*G'*) and (b) loss (*G"*) moduli measured at 90 ^{0}C for the neat SEO electrolyte, and salt-containing SEO electrolytes at r_{av} = 0.085 and r_{av} = 0.20. Error bars from the 3 repeated measurements for each sample are too small to be visible.

The results of electrochemical characterization experiments on this SEO electrolyte as a function of average salt concentration are shown in Figure 4. All electrochemical characterization was conducted at 90 ^{0}C, the temperature used throughout the protrusion growth study.

12

Figure 4(a) presents the ionic conductivity from ac impedance spectroscopy of symmetric cells with blocking electrodes, κ_b, and with non-blocking electrodes, κ_{nb}, as a function of the average salt concentration. Both κ_b and κ_{nb} follow the same trend. The ionic conductivity increases with r_{av} until a maximum is reached in the vicinity of $r_{av} = 0.085$. This is followed by a decrease at higher r_{av} values. This behavior is similar to many previous reports on the ionic conductivity of SEO electrolytes.[20,46–51] The solid curve represents a polynomial fit through the κ_b data; the polynomial is given in Figure 4(a). In order to reduce the influence of experimental noise on our analysis, fits of experimental data will be used.

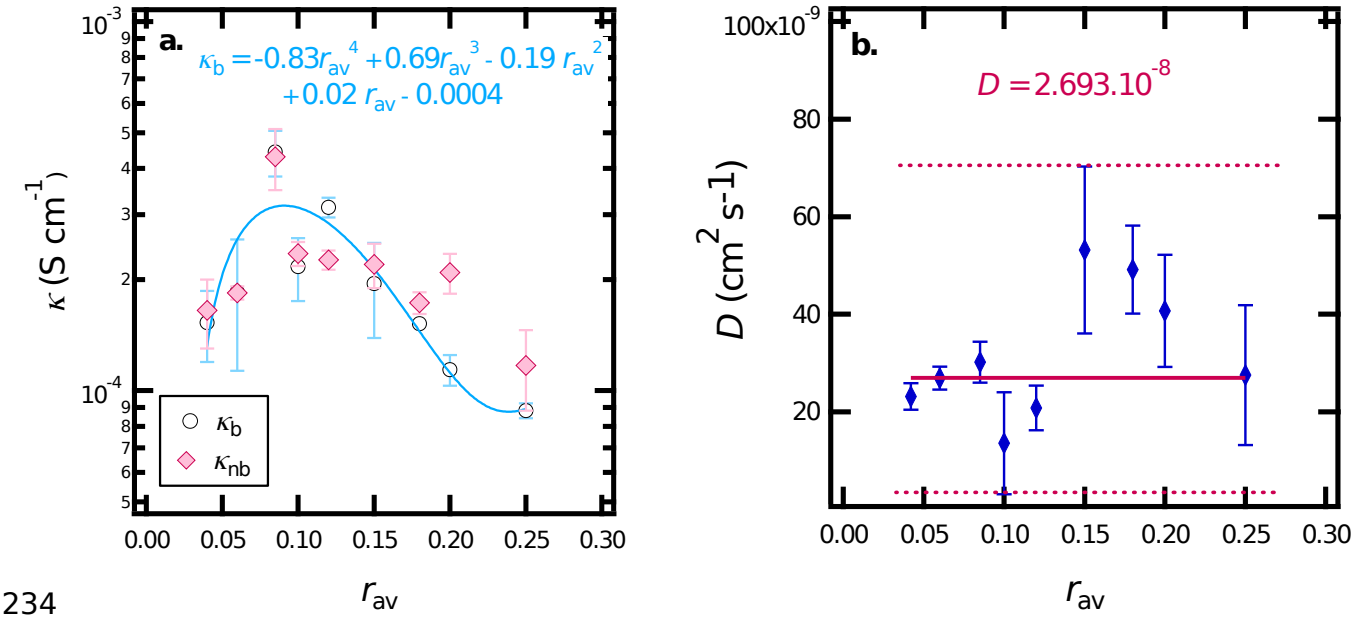

13

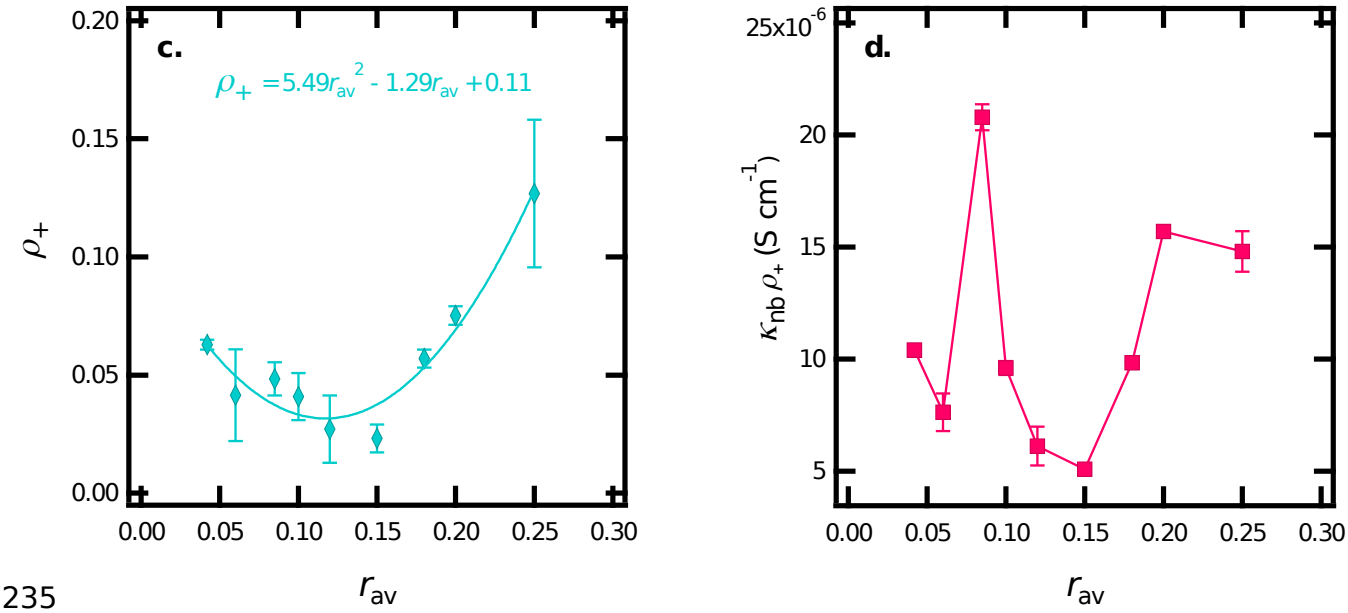

Figure 4. Electrochemical properties of SEO electrolytes at 90 ^{0}C as a function of salt concentration, r_{av}. (a) Ionic conductivity, κ, from ac impedance spectroscopy of symmetric cells with blocking electrodes, κ_b, and with non-blocking electrodes, κ_{nb}. (b) Salt diffusion coefficient, D, obtained by restricted diffusion in a Li/SEO/Li symmetric cell (diamonds represent the average measured diffusion coefficient). The solid line represents the average diffusion coefficient. The two dotted lines represent the upper and lower bounds of the experimental data including error bars. (c) Current fraction, ρ_+, obtained using the steady-state current technique in a Li/SEO/Li symmetric cell. Error bars in (a), (b), and (c) represent the standard deviation from 3 measurements. (d) Product of ionic conductivity, κ_{nb}, (Figure 4(a)) and steady-state current fraction, ρ_+ (Figure 4(c)). The error bars represent the standard errors calculated from the standard deviations of the measured κ_{nb} and ρ_+.

Figure 4(b) presents the salt diffusion coefficient, D, obtained by the restricted diffusion method, in Li/SEO/Li symmetric cells at 90 ^{0}C. The data are scattered around an average value

of 2.69 x 10^{-8} cm^2 s^{-1}, represented by the solid red line in Figure 4(b). These data are consistent with previous studies of SEO electrolytes.[48] For simplicity, we assume that D is independent of salt concentration. The dotted lines in Figure 4(b) represent the upper and lower bounds of the experimental data including error bars.

Figure 4(c) shows the current fraction, $\rho_{+¿¿}$, measured at 90 ºC, determined by the steady-state approach proposed by Bruce and Vincent.[38] This method gives the cation transference number for a thermodynamically ideal dilute electrolyte. The current fraction follows a parabolic trend with a minimum at $r_{av} = 0.15$, consistent with previous studies.[48,52] The solid turquoise curve in Figure 4(c) represents a quadratic fit.

The current obtained in a Li/SEO/Li symmetric cell in the limit of small applied fields is proportional to the product $\kappa_{nb}\ \rho_{+¿¿}$.[39,53–55] (For comparison, we show this product for both conductivity measured with blocking and non-blocking electrodes in Figure S3 in the SI.) This product is thus a measure of the efficacy of the electrolyte in the limit of infinitesimal current. In Figure 4(d) we plot $\kappa_{nb}\ \rho_{+¿¿}$ versus r_{av}. The dependence of $\kappa_{nb}\ \rho_{+¿¿}$ on r_{av} is non-monotonic with a sharp maximum on $r_{av} = 0.085$ and a relatively shallow maximum at $r_{av} = 0.20$.

Since we have already shown that the dependence of morphology and mechanical properties of our SEO electrolyte on average salt concentration cannot explain the cell cycling results in Figure 1, we are left with the conclusion that the electrochemical properties of the electrolyte must play a role. The data in Figure 4(b) indicate that cell lifetime is not affected by the salt diffusion coefficient alone, as the former is a strong function of average salt concentration and the latter is independent of average salt concentration. Similarly, the dependence of the efficacy

of SEO electrolytes, in the limit of small applied fields, on average salt concentration is very different from the dependence of cell lifetime on average salt concentration (Figure 4(d)). We thus examine other electrochemical characteristics of our SEO electrolytes.

Complete electrochemical characterization of an electrolyte requires knowledge of the transference number with respect to the solvent velocity, $t_{+¿^0¿}$,[48,56,57] and the thermodynamic factor, T_f. We use the method described in reference [57] to determine $t_{+¿^0¿}$ and T_f from the data presented in Figure 4. This method requires knowledge of the open circuit potential of the electrolyte in concentration cells. In reference [52], it was shown that the open circuit potential of many different SEO electrolytes was within experimental error (see Figure S3 in SI). We use this result to calculate $t_{+¿^0¿}$ and T_f of our SEO electrolyte as a function of r_{av}, and these results are given in Figure 5.

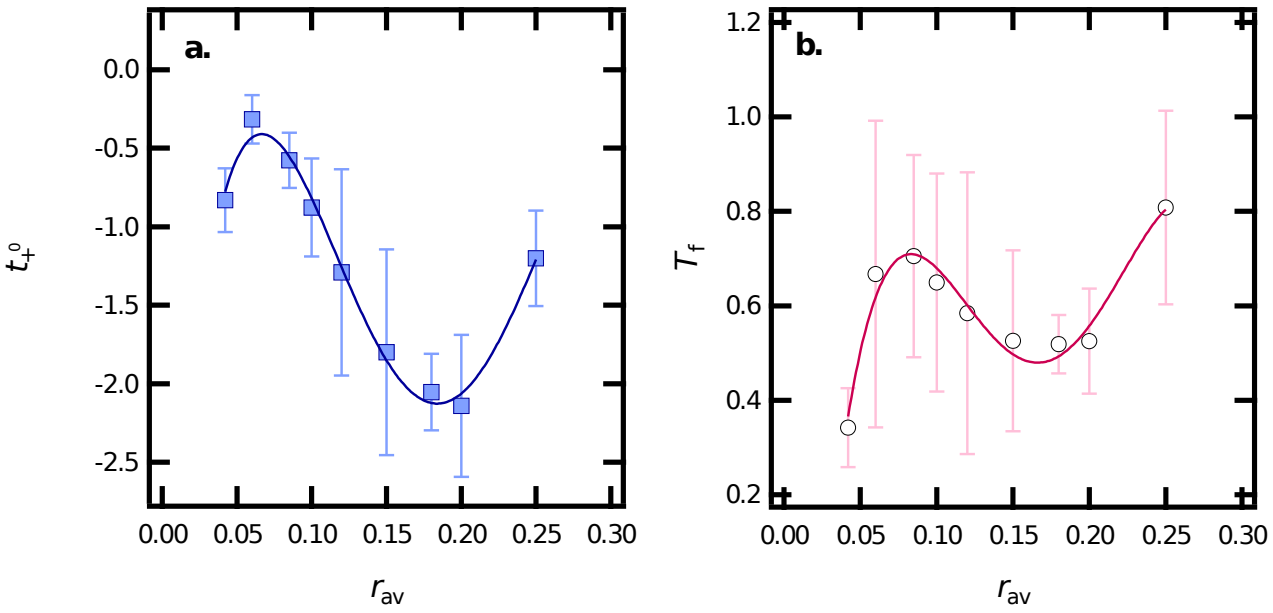

16

Figure 5. (a) Cation transference number with respect to the solvent velocity, $t_{+¿^0¿}$ and (b) thermodynamic factor $T_f = 1+\frac{dln\gamma_{\pm}}{dlnm}$. Fitted values from Figures 4(a), (b) and (c) are used to evaluate $t_{+¿^0¿}$ and T_f. Markers are the calculated data, error bars represent the standard errors calculated from the standard deviations of the measured properties, and dotted lines are polynomial fits.

Equations 4 and 5 were used to determine $t_{+¿^0¿}$ and T_f from experimental measurements.

$$t_{+¿^0=1+¿¿} \qquad \textit{Equation 4}$$

$$T_f=\left(1+\frac{dln\gamma_{\pm}}{dlnm}\right)=-¿¿¿ \qquad \textit{Equation 5}$$

where F is the Faraday constant (C mol), R is the gas constant (J mol^{-1} K^{-1}), c is the salt concentration (mol.cm^{-3}), ϕ_c is the volume fraction of the conducting phase, m is the molality (mol kg^{-1}), $\frac{dU}{dlnm}$ is the change in the open circuit potential, $z_{+¿¿}$is the charge number, $v_{+¿¿}$ is the number of cations, both $z_{+¿¿}$ and $v_{+¿¿}$are 1 for LiTFSI, and $v=v_{+¿+v_{-¿¿¿}$.

We used fitted functions for the concentration dependent parameters on the right-hand side of Equations 4 and 5 to obtain $t_{+¿^0¿}$ and T_f: the solid curves in Figures 4(a) and (c) and the horizontal line in Figure 4(b).

The cation transference number is negative over the entire range of average salt concentration, varying from -0.31 to -2.14 (Figure 5(a)). It is a non-monotonic function of average salt concentration with a maximum at r_{av} = 0.06 and a minimum at r_{av} = 0.20. The thermodynamic factor, shown in Figure 5(b), varies between 0.34 and 0.8. If the electrolyte were

17

thermodynamically ideal, T_f would be unity at all average salt concentrations. Even at very low average salt concentrations, our electrolytes are far from ideal.[46,48,57]

It is instructive to examine the salt concentration gradients that emerge in our electrolyte at i = 0.175 mA cm^{-2}. These gradients depend on all of the transport and thermodynamic parameters discussed in Figures 4 and 5. The importance of salt concentration gradients has been recognized by several researchers.[14,58] We used the methodology developed by Pesko *et al.*[31] to calculate r(x), the salt concentration profile at steady state which is given by

$$\int_{r(x=0)}^{r(x)} \frac{D(r)c(r)}{r\,t_{-}^{0}(r)}dr = \int_{r(x=0)}^{r(x)} J(r)dr = \frac{-iL}{F}\left(\frac{x}{L}\right)\text{¿}, \qquad \textit{Equation 6}$$

where $c(r)$ is the molar salt concentration, and the anion transference number, t_{-}^{0}, is defined as 1 - t_{+}^{0}.

Furthermore, substituting t_{-}^{0} by its equivalent using Equation 4 in $J(r)$, we can rewrite Equation 6 as:

$$J(r) = \frac{\kappa}{\text{¿}\,\text{¿}} \qquad \textit{Equation 7}$$

The integrand on the left side of equation 6 contains two parameters D(r) and t_{-}^{0}. It is important to recognize that t_{-}^{0} (or equivalently t_{+}^{0}) is not measured directly but requires combining measurements of ρ_{+} with κ, D and $\frac{d\,U}{d\ln m}$ (see Equation 4). The experimental uncertainty of t_{-}^{0} is thus compounded by the experimental uncertainty of 4 independently measured parameters. In contrast, the 3 parameters given in Equation 7, ρ_{+}, κ and $\frac{d\,U}{d\ln m}$ are all measured directly. Equation 7 also makes it clear that the current, i, is not dependent on D, and

this arises because t_{-} is proportional to D. Equation 6 and 7 are based on the framework presented in [30]. For the case of thermodynamically ideal dilute electrolytes, these equations reduce to the familiar result of Bruce and Vincent in the limit of small salt concentration.[38]

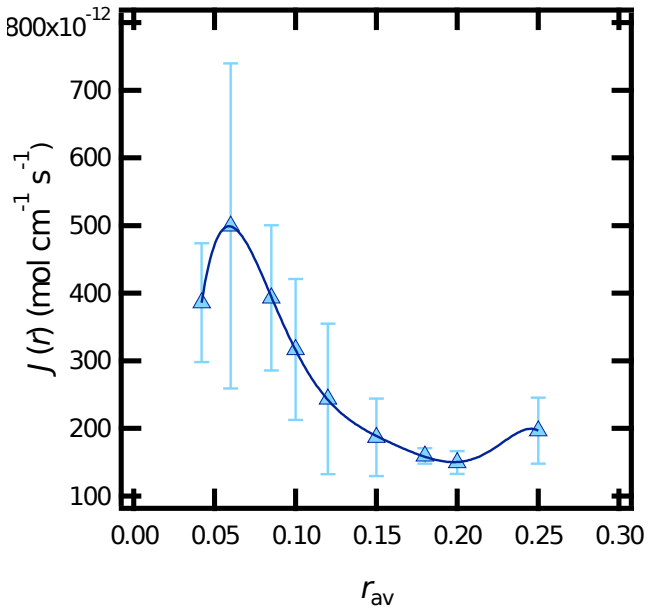

Figure 6. Dependence of $J(r)$ on salt concentration, r_{av}, at 90 ^{0}C. The dashed curve shows the least-squares polynomial fit. Error bars show the standard error calculated from the standard deviations of the measured electrochemical parameters.

The integrand, $J(r)$, is a known function of salt concentration r_{av}. We plot this function in Figure 6. A polynomial fit was used to calculate the required integral. The dashed curve shows a polynomial fit of Equation 7:

$$J(r) = ar_{av}^6 + br_{av}^5 + cr_{av}^4 + dr_{av}^3 + er_{av}^2 + fr_{av} + g, \qquad \textit{Equation 8}$$

with fitting parameters a = -4 x 10^{-4}, b = 4 x 10^{-4}, c = -1 x 10^{-4}, d = 3 x 10^{-5}, e = -3 x 10^{-6}, f = 2 x 10^{-7}, and g = -3 x 10^{-9}. Our goal is to establish $r(x)$ for a given value of r_{av} and i. This is achieved

19

by first assuming $r(x = 0)$ and solving for $r(x)$ using Equation 7 for all x from 0^+ to L by numerical integration.

Figure 7(a) presents the salt concentration profile at steady state for all salt concentrations at a current density of 0.02 mA cm^{-2}, the current density used during the conditioning cycles. Figure 7(b) presents the salt concentration profile at steady state for all salt concentrations at a current density of 0.175 mA cm^{-2}, the current density used during in our study of protrusion growth. For both sets of calculations, the electrolyte thickness was assumed to be 0.005 cm. As expected, increasing current density results in steeper concentration gradients. The magnitude of the gradients also increases with average salt concentration. This is seen more clearly in Figure 7(b).

20

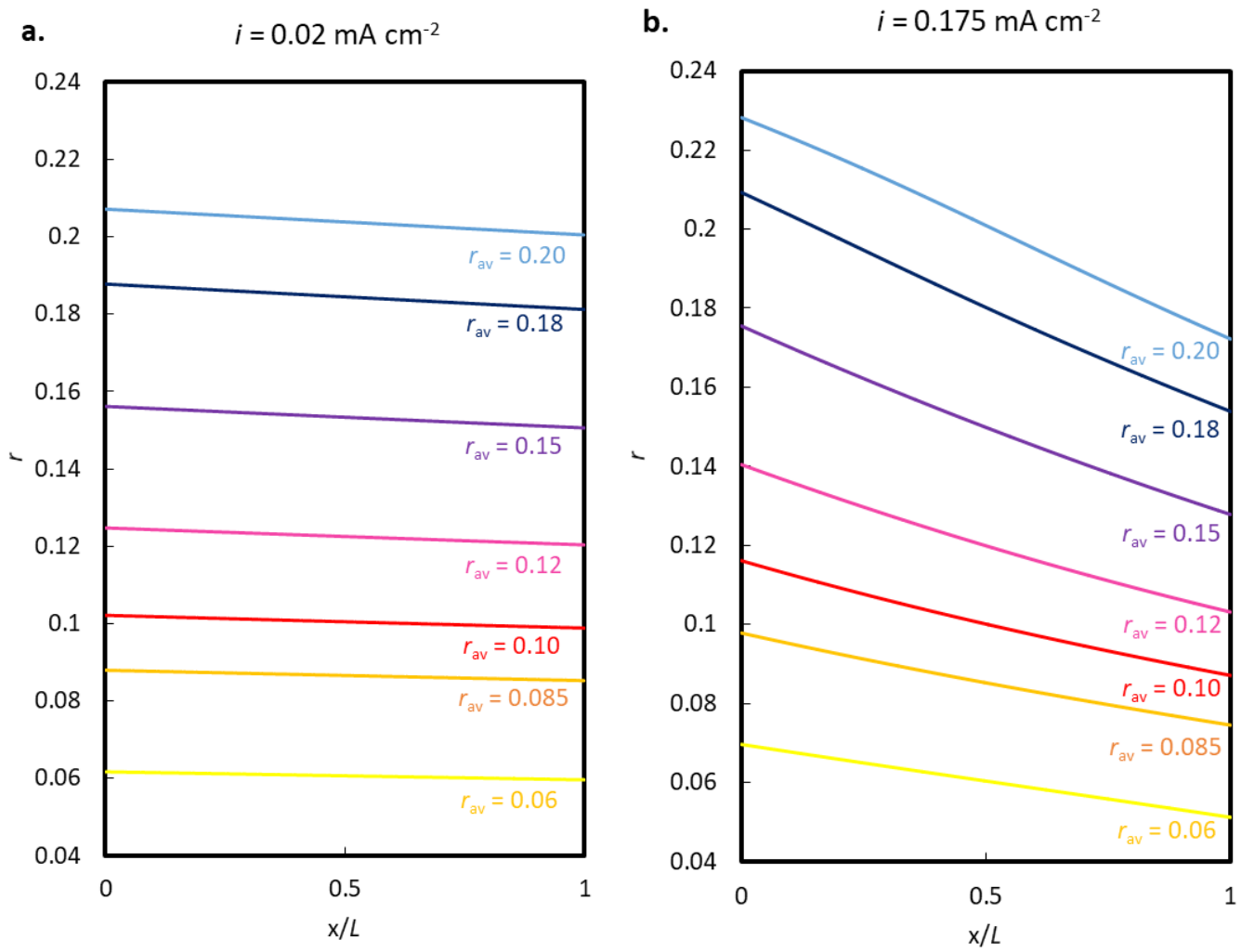

343

344 **Figure 7.** Concentration profiles in SEO electrolytes predicted by concentrated solution theory at
345 steady-state at 90 ^{o}C. (a) Concentration profiles for i = 0.02 mA cm^{-2}, the current density used
346 during conditioning cycles. (b) Concentration profiles for i = 0.175 mA cm^{-2}, the current density
347 used in our study of protrusion growth during cell cycling. The anode is at x/L = 0 and the
348 cathode is at x/L = 1.

349 In order to quantify differences in salt concentration profiles (Figure 7), we define an average
350 salt concentration gradient, Δ, to be the difference of salt concentration between the anode and
351 cathode electrodes, divided by the thickness of the cell. Figure 8 presents the calculated salt

21

concentration gradients as a function of average salt concentration for the two current densities of interest. During the conditioning cycles (blue squares), salt concentration gradients are small, varying from 0.4 cm^{-1} for r_{av} = 0.06 to 1.3 cm^{-1} for r_{av} = 0.20. However, for the higher current density (turquoise circles), the gradients are large and about 10 times higher than that during the conditioning cycles. One may use the magnitude of Δ as a measure of the efficacy of an electrolyte at the current density of interest. The magnitude of the salt concentration gradient to maintain a current density of i = 0.175 mA cm^{-2} increases monotonically with salt concentration. Many theories[59,60] suggest that lithium dendrite growth is affected by the magnitude of salt concentration gradients. It is therefore instructive to examine the cycling behavior of our cells as a function of Δ.

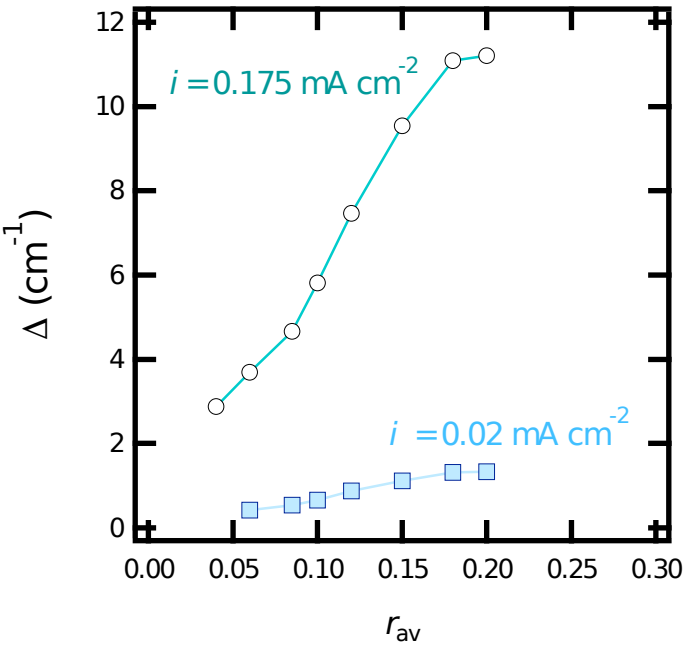

Figure 8. A plot of average salt concentration gradient at 90 ^{0}C, Δ, defined as the salt concentration difference between the cathode and the anode normalized by electrolyte thickness, as a function of the average salt concentration, r_{av}, for current density used in the conditioning

22

cycles at i = 0.02 mA cm^{-2} (turquoise circles) and for current density used in our study of protrusion growth during cell cycling at i = 0.175 mA cm^{-2} (blue squares).

In Figure 9(a) we plot cell lifetime as a function of Δ. We see a direct correlation between the two parameters. Cell lifetime decreases precipitously as Δ increases from 2.8 cm^{-1} to 9.5 cm^{-1}. The average salt concentrations used to obtain each of the data points is indicated using the color scheme shown on the right. Cell lifetimes obtained at the two highest values of Δ are slightly higher than that at 9.5 cm^{-1}, an observation that requires further investigation. Nevertheless, the data in Figure 9(a) indicate that Δ must be significantly less than 9 cm^{-1} for stable cycling of lithium-lithium symmetric cells. We note in passing that Δ for the conditioning cycles ranges from 0.4 to 1.3 cm^{-1}. This range is well outside the range of gradients where rapid cell failure is expected. Planar and stable deposition might be expected in this range as seen by Maslyn *et al.* [28]

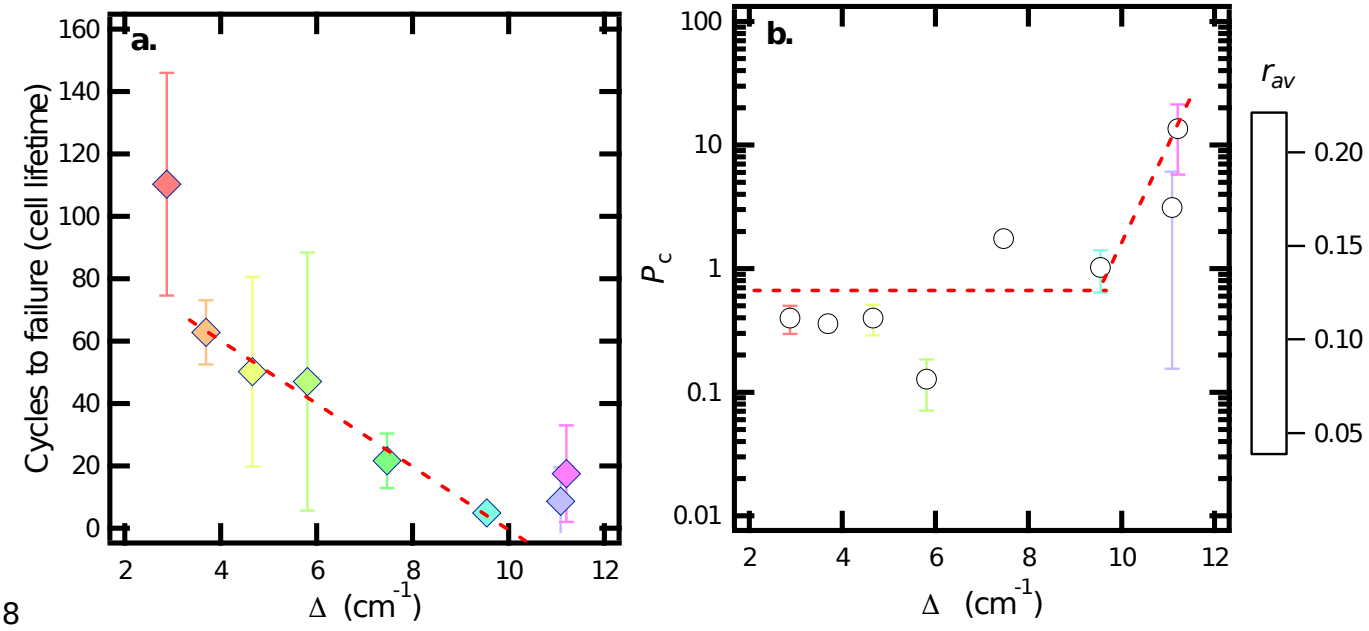

23

Figure 9. (a) Cell lifetime (cycles to failure) and (b) average number of defects per cycle, P_c, as a function of salt concentration gradient, Δ at 90 ^{0}C. Data points are color-coded according to salt concentration, r_{av}, using the color scale presented on the right. Dashed lines are guides for the eye.

An important characteristic of failed cells is the areal density of defects on the electrodes at the point of failure. Since different cells exhibited different lifetimes, it makes sense to examine the average number of defects per cycle P_c, in all of the failed cells. The procedure for quantifying P_c is presented in ref.[29] In Figure 9(b), we plot P_c versus Δ. To a good approximation, P_c is independent of Δ when Δincreases from 2.8 cm^{-1} to 9.5 cm^{-1}, suggesting that areal defect density in this regime is related to an intrinsic property of lithium metal rather than the applied current. Note that cell lifetime decreases rapidly over the same range of Δ values. In the regime Δ > 9.5 cm^{-1}, P_c increases substantially with Δ, suggesting that defects density in this regime is affected by the applied current. Many of the defects seen at high salt concentration do not protrude significantly into the electrolyte (see Figure S5 in the SI). Since cell-failure requires a protrusion to span the thickness of the electrolyte, our experiments do not shed light on the effect of these defects on cell-failure.

CONCLUSION

We have studied both the failure of cycled Li/SEO/Li symmetric cells due to the defective electrodeposition of lithium and the formation of lithium protrusions as a function of salt concentration in the SEO electrolyte (r_{av}) at a fixed current density. The SEO electrolyte presents a lamellar morphology at all salt concentrations. We find that the cell lifetime decreases by a factor of 100 when salt concentration in the SEO electrolyte is increased from r_{av}=¿0.04 to 0.15,

and it remains low at the highest salt concentrations tested. The average number of defective deposits on the electrodes is also considerably higher at high salt concentrations. We know that the defective electrodeposition of lithium is controlled by electrochemical and mechanical properties of the electrolyte. Since these properties depend on the morphology of the electrolyte, we first studied the effect of salt on electrolyte morphology. We found no qualitative differences in the morphology as a function of salt concentration. We also found no significant difference in the mechanical properties as a function of r_{av}. The electrochemical properties were quantified by measuring the ionic conductivity, salt diffusion coefficient, transference number, and thermodynamic factor. None of these properties deteriorated rapidly with increasing salt concentration. We used these properties to compute salt concentration profiles in the symmetric cells using Newman's concentrated solution theory. We posit that Δ, the average salt concentration gradient across the electrolyte, governs protrusion growth from a lithium metal cathode through an electrolyte. We show that cell lifetime decreases linearly with Δ.

Since the early work by Monroe and Newman,[24,44,45] it has been clear that the growth of lithium protrusions is related to the electrochemical and mechanical properties of the electrolyte. Which of these properties is directly relevant for the observed protrusions has not yet been established. It is common to report parameters such as modulus, conductivity, and transference number. These parameters characterize the linear response of the electrolyte as they are relevant when the electrolyte is slightly perturbed away from equilibrium. The shear modulus describes stress-strain behavior in the limit of infinitesimal strain, conductivity describes the voltage-current relationship in the limit of infinitesimal current densities, and the transference number describes the migration of ions at uniform concentration. In this work, we have shown that cell

25

lifetime and protrusion density are not dependent on these parameters. Instead, we find that cell lifetime and protrusion density appear to be correlated with the concentration gradient, Δ, a parameter that reflects the nonlinear response of the electrolyte to the applied current density used in the cycling experiments. It would be interesting to see if the relationship between lithium protrusion growth and electrochemical properties in different classes of electrolytes can be understood in term of Δ.

ASSOCIATED CONTENT

The following file is available free of charge.

Supplementary Information (PDF)

AUTHOR INFORMATION

Corresponding Author

* E-mail: nbalsara@berkeley.edu. Phone: 1-510-642-8973

* Address: 201C Gilman Hall, Berkeley, CA 94720

ORCID

Louise Frenck: 0000-0001-7116-2144
Vijay D. Veeraraghavan: 0000-0001-7327-7316
Jacqueline A. Maslyn: 0000-0002-6481-2070
Alexander Müller: 0000-0002-8049-6610
Alec S. Ho: 0000-0003-1373-5332
Whitney S. Loo: 0000-0002-9773-3571
Andrew M. Minor: 0000-0003-3606-8309
Nitash P. Balsara: 0000-0002-0106-5565

Author Contributions

J.A.M. and W.S.L. synthesized SEO block copolymer. L.F., J.A.M., and V.V. fabricated samples and performed the experiments. A. M. acquired scanning electron micrographs. A.S.H. contributed to calculations. L.F. and N.P.B. prepared figures and composed the manuscript. N.P.B. directed the work.

26

Notes

The authors declare no competing financial interest.

ACKNOWLEDGMENT

Funding to support this work was provided by the Energy & Biosciences Institute through the EBI-Shell program. J.A.M. was supported by a National Science Foundation Graduate Research Fellowship DGE-2752814. Program. Funding for the electron microscopy work was provided by the Soft Matter Electron Microscopy Program, supported by the Office of Science, Office of Basic Energy Science, U.S. Department of Energy, under Contract No. DEAC02-05CH11231. Work at the Molecular Foundry was supported by the Office of Science, Office of Basic Energy Sciences, of the U.S. Department of Energy under Contract No. DE-AC02-05CH11231. A.S.H. was supported by the Vehicle Technologies Office of the U.S. Department of Energy's Office of Energy Efficiency and Renewable Energy under the guidance of the Advanced Battery Cell Research Program (eXtreme fast charge Cell Evaluation of Lithium-ion batteries, XCEL). W.S.L. was supported by a National Science Foundation Graduate Research Fellowship DGE-1106400. We acknowledge helpful discussions with Dr. Ryan Stephens of Shell International Exploration and Production Inc, Houston.

LIST OF SYMBOLS

C_d, Charge density passed (C.cm^{-2}); Δ, salt concentration gradient; d, Domain spacing (nm); D, restricted salt diffusion coefficient; $\frac{dU}{d\ln m}$, change in the open circuit potential; ΔV, potential applied (V); F, Faraday constant (G', Storage shear modulus; G'', loss shear modulus; i,

Applied current density (mA cm^{-2}); i_0, measured initial current (A); i_Ω, calculated initial current (A); κ_b, ionic conductivity from measurements with blocking electrodes ($S.cm^{-1}$); κ_{nb}, ionic conductivity from measurements with non-blocking electrodes ($S\ cm^{-1}$); *L*, electrolyte thickness; *Li*, Lithium; *Li-ion*, Lithium-ion battery; *LiTFSI*, Lithium bis (trifluoromethanesulfonyl) imide; *m*, molality (mol kg^{-1}); *NMP*, N-methylpyrrolidone; ρ_+, steady-state current fraction; ϕ_c, volume fraction of the conducting phase; P_c, average number of defects per cycle; *PEO*, Poly(ethylene oxide); *PS*, Polystyrene; *R*, gas constant ($J\ mol^{-1}\ K^{-1}$); r_{av}, Average salt concentration; $R_{b,0}$, initial bulk resistance (Ω); $R_{i,0}$, initial interfacial resistance (Ω); $R_{i,SS}$, interfacial resistance at steady state (Ω); *SEI*, Solid Electrolyte Interphase; *SEO*, Polystyrene-*b*-poly(ethylene) oxide; *T*, temperature; $t_{+¿^0¿}$, cation transference number; $t_{-¿^0¿}$, anion transference number; T_f, thermodynamic factor; *U*, open-circuit voltage (V); $v_{+¿¿}$, number of cations for LiTFSI; $z_{+¿¿}$, the charge number for LiTFSI.

REFERENCES

[1] J. Yamaki, S. Tobishima, K. Hayashi, Keiichi Saito, Y. Nemoto, M. Arakawa, A consideration of the morphology of electrochemically deposited lithium in an organic electrolyte, Journal of Power Sources. 74 (1998) 219–227. https://doi.org/10.1016/S0378-7753(98)00067-6.

[2] Y. Takeda, O. Yamamoto, N. Imanishi, Lithium Dendrite Formation on a Lithium Metal Anode from Liquid, Polymer and Solid Electrolytes, Electrochemistry. 84 (2016) 210–218. https://doi.org/10.5796/electrochemistry.84.210.

[3] K.N. Wood, E. Kazyak, A.F. Chadwick, K.-H. Chen, J.-G. Zhang, K. Thornton, N.P. Dasgupta, Dendrites and Pits: Untangling the Complex Behavior of Lithium Metal Anodes through Operando Video Microscopy, ACS Cent. Sci. 2 (2016) 790–801. https://doi.org/10.1021/acscentsci.6b00260.

[4] E.J. Cheng, A. Sharafi, J. Sakamoto, Intergranular Li metal propagation through polycrystalline Li6.25Al0.25La3Zr2O12 ceramic electrolyte, Electrochimica Acta. 223 (2017) 85–91. https://doi.org/10.1016/j.electacta.2016.12.018.

[5] L. Frenck, G.K. Sethi, J.A. Maslyn, N.P. Balsara, Factors That Control the Formation of Dendrites and Other Morphologies on Lithium Metal Anodes, Front. Energy Res. 7 (2019). https://doi.org/10.3389/fenrg.2019.00115.

28

[6] M.M. Thackeray, C. Wolverton, E.D. Isaacs, Electrical energy storage for transportation—approaching the limits of, and going beyond, lithium-ion batteries, Energy Environ. Sci. 5 (2012) 7854–7863. https://doi.org/10.1039/C2EE21892E.
[7] D. Aurbach, E. Zinigrad, Y. Cohen, H. Teller, A short review of failure mechanisms of lithium metal and lithiated graphite anodes in liquid electrolyte solutions, Solid State Ionics. 148 (2002) 405–416. https://doi.org/10.1016/S0167-2738(02)00080-2.
[8] P.G. Bruce, S.A. Freunberger, L.J. Hardwick, J.-M. Tarascon, Li–O 2 and Li–S batteries with high energy storage, Nature Materials. 11 (2012) 19–29. https://doi.org/10.1038/nmat3191.
[9] D. Lin, Y. Liu, Y. Cui, Reviving the lithium metal anode for high-energy batteries, Nature Nanotechnology. 12 (2017) 194–206. https://doi.org/10.1038/nnano.2017.16.
[10] K.N. Wood, M. Noked, N.P. Dasgupta, Lithium Metal Anodes: Toward an Improved Understanding of Coupled Morphological, Electrochemical, and Mechanical Behavior, ACS Energy Lett. 2 (2017) 664–672. https://doi.org/10.1021/acsenergylett.6b00650.
[11] C. Brissot, M. Rosso, J.-N. Chazalviel, S. Lascaud, Dendritic growth mechanisms in lithium/polymer cells, Journal of Power Sources. 81–82 (1999) 925–929. https://doi.org/10.1016/S0378-7753(98)00242-0.
[12] C. Brissot, M. Rosso, J.-N. Chazalviel, P. Baudry, S. Lascaud, In situ study of dendritic growth inlithium/PEO-salt/lithium cells, Electrochimica Acta. 43 (1998) 1569–1574. https://doi.org/10.1016/S0013-4686(97)10055-X.
[13] A. Teyssot, C. Belhomme, R. Bouchet, M. Rosso, S. Lascaud, M. Armand, Inter-electrode in situ concentration cartography in lithium/polymer electrolyte/lithium cells, Journal of Electroanalytical Chemistry. 584 (2005) 70–74. https://doi.org/10.1016/j.jelechem.2005.01.037.
[14] M. Rosso, J.-N. Chazalviel, E. Chassaing, Calculation of the space charge in electrodeposition from a binary electrolyte, Journal of Electroanalytical Chemistry. 587 (2006) 323–328. https://doi.org/10.1016/j.jelechem.2005.11.030.
[15] P. Barai, K. Higa, V. Srinivasan, Effect of Initial State of Lithium on the Propensity for Dendrite Formation: A Theoretical Study, J. Electrochem. Soc. 164 (2017) A180–A189. https://doi.org/10.1149/2.0661702jes.
[16] P. Barai, K. Higa, V. Srinivasan, Impact of External Pressure and Electrolyte Transport Properties on Lithium Dendrite Growth, J. Electrochem. Soc. 165 (2018) A2654–A2666. https://doi.org/10.1149/2.0651811jes.
[17] J.-M. Tarascon, M. Armand, Issues and challenges facing rechargeable lithium batteries, Nature. (2001). https://doi.org/10.1038/35104644.
[18] A. Lisowska-Oleksiak, The interface between lithium and poly(ethylene-oxide), Solid State Ionics. 119 (1999) 205–209. https://doi.org/10.1016/S0167-2738(98)00504-9.
[19] M. Armand, The history of polymer electrolytes, Solid State Ionics. 69 (1994) 309–319. https://doi.org/10.1016/0167-2738(94)90419-7.
[20] R. Bouchet, S. Maria, R. Meziane, A. Aboulaich, L. Lienafa, J.-P. Bonnet, T.N.T. Phan, D. Bertin, D. Gigmes, D. Devaux, R. Denoyel, M. Armand, Single-ion BAB triblock copolymers as highly efficient electrolytes for lithium-metal batteries, Nature Materials. 12 (2013) 452–457. https://doi.org/10.1038/nmat3602.

[21] D. Xu, B. Wang, Q. Wang, S. Gu, W. Li, J. Jin, C. Chen, Z. Wen, High-Strength Internal Cross-Linking Bacterial Cellulose-Network-Based Gel Polymer Electrolyte for Dendrite-Suppressing and High-Rate Lithium Batteries, ACS Appl. Mater. Interfaces. 10 (2018) 17809–17819. https://doi.org/10.1021/acsami.8b00034.
[22] D. Li, L. Chen, T. Wang, L.-Z. Fan, 3D Fiber-Network-Reinforced Bicontinuous Composite Solid Electrolyte for Dendrite-free Lithium Metal Batteries, ACS Appl. Mater. Interfaces. 10 (2018) 7069–7078. https://doi.org/10.1021/acsami.7b18123.
[23] J. Hu, J. Tian, C. Li, Nanostructured Carbon Nitride Polymer-Reinforced Electrolyte To Enable Dendrite-Suppressed Lithium Metal Batteries, ACS Appl. Mater. Interfaces. 9 (2017) 11615–11625. https://doi.org/10.1021/acsami.7b00478.
[24] C. Monroe, J. Newman, Dendrite Growth in Lithium/Polymer Systems A Propagation Model for Liquid Electrolytes under Galvanostatic Conditions, J. Electrochem. Soc. 150 (2003) A1377–A1384. https://doi.org/10.1149/1.1606686.
[25] Y. Yamada, M. Yaegashi, T. Abe, A. Yamada, A superconcentrated ether electrolyte for fast-charging Li-ion batteries, Chem. Commun. 49 (2013) 11194–11196. https://doi.org/10.1039/C3CC46665E.
[26] Y. Yamada, J. Wang, S. Ko, E. Watanabe, A. Yamada, Advances and issues in developing salt-concentrated battery electrolytes, Nature Energy. 4 (2019) 269–280. https://doi.org/10.1038/s41560-019-0336-z.
[27] N.S. Schauser, K.J. Harry, D.Y. Parkinson, H. Watanabe, N.P. Balsara, Lithium Dendrite Growth in Glassy and Rubbery Nanostructured Block Copolymer Electrolytes, J. Electrochem. Soc. 162 (2015) A398–A405. https://doi.org/10.1149/2.0511503jes.
[28] J.A. Maslyn, W.S. Loo, K.D. McEntush, H.J. Oh, K.J. Harry, D.Y. Parkinson, N.P. Balsara, Growth of Lithium Dendrites and Globules through a Solid Block Copolymer Electrolyte as a Function of Current Density, J. Phys. Chem. C. 122 (2018) 26797–26804. https://doi.org/10.1021/acs.jpcc.8b06355.
[29] L. Frenck, J.A. Maslyn, W.S. Loo, D.Y. Parkinson, N.P. Balsara, Impact of Salt Concentration on Nonuniform Lithium Electrodeposition through Rigid Block Copolymer Electrolytes, ACS Appl. Mater. Interfaces. (2019). https://doi.org/10.1021/acsami.9b15606.
[30] Newman, J.; Thomas-Alya, K. E., *Electrochemical Systems, 3rd Edition | Wiley, 2004.*
[31] D.M. Pesko, Z. Feng, S. Sawhney, J. Newman, V. Srinivasan, N.P. Balsara, Comparing Cycling Characteristics of Symmetric Lithium-Polymer-Lithium Cells with Theoretical Predictions, J. Electrochem. Soc. 165 (2018) A3186–A3194. https://doi.org/10.1149/2.0921813jes.
[32] P.G. Bruce, C.A. Vincent, Polymer electrolytes, J. Chem. Soc., Faraday Trans. 89 (1993) 3187–3203. https://doi.org/10.1039/FT9938903187.
[33] M. Singh, O. Odusanya, G.M. Wilmes, H.B. Eitouni, E.D. Gomez, A.J. Patel, V.L. Chen, M.J. Park, P. Fragouli, H. Iatrou, N. Hadjichristidis, D. Cookson, N.P. Balsara, Effect of Molecular Weight on the Mechanical and Electrical Properties of Block Copolymer Electrolytes, Macromolecules. 40 (2007) 4578–4585. https://doi.org/10.1021/ma0629541.
[34] S.A. Mullin, G.M. Stone, A. Panday, N.P. Balsara, Salt Diffusion Coefficients in Block Copolymer Electrolytes, J. Electrochem. Soc. 158 (2011) A619–A627. https://doi.org/10.1149/1.3563802.

[35] K.J. Harry, D.T. Hallinan, D.Y. Parkinson, A.A. MacDowell, N.P. Balsara, Detection of subsurface structures underneath dendrites formed on cycled lithium metal electrodes, Nature Materials. 13 (2014) 69–73. https://doi.org/10.1038/nmat3793.
[36] K.J. Harry, X. Liao, D.Y. Parkinson, A.M. Minor, N.P. Balsara, Electrochemical Deposition and Stripping Behavior of Lithium Metal across a Rigid Block Copolymer Electrolyte Membrane, J. Electrochem. Soc. 162 (2015) A2699–A2706. https://doi.org/10.1149/2.0321514jes.
[37] K.J. Harry, K. Higa, V. Srinivasan, N.P. Balsara, Influence of Electrolyte Modulus on the Local Current Density at a Dendrite Tip on a Lithium Metal Electrode, J. Electrochem. Soc. 163 (2016) A2216–A2224. https://doi.org/10.1149/2.0191610jes.
[38] P.G. Bruce, C.A. Vincent, Steady state current flow in solid binary electrolyte cells, Journal of Electroanalytical Chemistry and Interfacial Electrochemistry. 225 (1987) 1–17. https://doi.org/10.1016/0022-0728(87)80001-3.
[39] M.D. Galluzzo, J.A. Maslyn, D.B. Shah, N.P. Balsara, Ohm's law for ion conduction in lithium and beyond-lithium battery electrolytes, J. Chem. Phys. 151 (2019) 020901. https://doi.org/10.1063/1.5109684.
[40] E.W. Cochran, C.J. Garcia-Cervera, G.H. Fredrickson, Stability of the Gyroid Phase in Diblock Copolymers at Strong Segregation, Macromolecules. 39 (2006) 2449–2451. https://doi.org/10.1021/ma0527707.
[41] F.S. Bates, J.H. Rosedale, G.H. Fredrickson, Fluctuation effects in a symmetric diblock copolymer near the order–disorder transition, J. Chem. Phys. 92 (1990) 6255–6270. https://doi.org/10.1063/1.458350.
[42] A. Panday, S. Mullin, E.D. Gomez, N. Wanakule, V.L. Chen, A. Hexemer, J. Pople, N.P. Balsara, Effect of Molecular Weight and Salt Concentration on Conductivity of Block Copolymer Electrolytes, Macromolecules. 42 (2009) 4632–4637. https://doi.org/10.1021/ma900451e.
[43] G.M. Stone, S.A. Mullin, A.A. Teran, D.T. Hallinan, A.M. Minor, A. Hexemer, N.P. Balsara, Resolution of the Modulus versus Adhesion Dilemma in Solid Polymer Electrolytes for Rechargeable Lithium Metal Batteries, J. Electrochem. Soc. 159 (2012) A222–A227. https://doi.org/10.1149/2.030203jes.
[44] C. Monroe, J. Newman, The Effect of Interfacial Deformation on Electrodeposition Kinetics, J. Electrochem. Soc. 151 (2004) A880–A886. https://doi.org/10.1149/1.1710893.
[45] C. Monroe, J. Newman, The Impact of Elastic Deformation on Deposition Kinetics at Lithium/Polymer Interfaces, J. Electrochem. Soc. 152 (2005) A396–A404. https://doi.org/10.1149/1.1850854.
[46] Y. Ma, M. Doyle, T.F. Fuller, M.M. Doeff, L.C.D. Jonghe, J. Newman, The Measurement of a Complete Set of Transport Properties for a Concentrated Solid Polymer Electrolyte Solution, J. Electrochem. Soc. 142 (1995) 1859–1868. https://doi.org/10.1149/1.2044206.
[47] K.I.S. Mongcopa, M. Tyagi, J.P. Mailoa, G. Samsonidze, B. Kozinsky, S.A. Mullin, D.A. Gribble, H. Watanabe, N.P. Balsara, Relationship between Segmental Dynamics Measured by Quasi-Elastic Neutron Scattering and Conductivity in Polymer Electrolytes, ACS Macro Lett. 7 (2018) 504–508. https://doi.org/10.1021/acsmacrolett.8b00159.
[48] I. Villaluenga, D.M. Pesko, K. Timachova, Z. Feng, J. Newman, V. Srinivasan, N.P. Balsara, Negative Stefan-Maxwell Diffusion Coefficients and Complete Electrochemical

Transport Characterization of Homopolymer and Block Copolymer Electrolytes, J. Electrochem. Soc. 165 (2018) A2766–A2773. https://doi.org/10.1149/2.0641811jes.
[49] W.-S. Young, W.-F. Kuan, T.H. Epps, Block copolymer electrolytes for rechargeable lithium batteries, Journal of Polymer Science Part B: Polymer Physics. 52 (2014) 1–16. https://doi.org/10.1002/polb.23404.
[50] W.-S. Young, T.H. Epps, Ionic Conductivities of Block Copolymer Electrolytes with Various Conducting Pathways: Sample Preparation and Processing Considerations, Macromolecules. 45 (2012) 4689–4697. https://doi.org/10.1021/ma300362f.
[51] Y. Gu, S. Zhang, L. Martinetti, K.H. Lee, L.D. McIntosh, C.D. Frisbie, T.P. Lodge, High Toughness, High Conductivity Ion Gels by Sequential Triblock Copolymer Self-Assembly and Chemical Cross-Linking, J. Am. Chem. Soc. 135 (2013) 9652–9655. https://doi.org/10.1021/ja4051394.
[52] M.D. Galluzzo, W.S. Loo, A.A. Wang, A. Walton, J.A. Maslyn, N.P. Balsara, Measurement of Three Transport Coefficients and the Thermodynamic Factor in Block Copolymer Electrolytes with Different Morphologies, J. Phys. Chem. B. (2020). https://doi.org/10.1021/acs.jpcb.9b11066.
[53] Q. Zheng, D.M. Pesko, B.M. Savoie, K. Timachova, A.L. Hasan, M.C. Smith, T.F. Miller, G.W. Coates, N.P. Balsara, Optimizing Ion Transport in Polyether-Based Electrolytes for Lithium Batteries, Macromolecules. 51 (2018) 2847–2858. https://doi.org/10.1021/acs.macromol.7b02706.
[54] Y. Tominaga, K. Yamazaki, V. Nanthana, Effect of Anions on Lithium Ion Conduction in Poly(ethylene carbonate)-based Polymer Electrolytes, J. Electrochem. Soc. 162 (2015) A3133–A3136. https://doi.org/10.1149/2.0211502jes.
[55] D.B. Shah, K.R. Olson, A. Karny, S.J. Mecham, J.M. DeSimone, N.P. Balsara, Effect of Anion Size on Conductivity and Transference Number of Perfluoroether Electrolytes with Lithium Salts, J. Electrochem. Soc. 164 (2017) A3511–A3517. https://doi.org/10.1149/2.0301714jes.
[56] N.P. Balsara, J. Newman, Relationship between Steady-State Current in Symmetric Cells and Transference Number of Electrolytes Comprising Univalent and Multivalent Ions, J. Electrochem. Soc. 162 (2015) A2720–A2722. https://doi.org/10.1149/2.0651514jes.
[57] D.M. Pesko, K. Timachova, R. Bhattacharya, M.C. Smith, I. Villaluenga, J. Newman, N.P. Balsara, Negative Transference Numbers in Poly(ethylene oxide)-Based Electrolytes, J. Electrochem. Soc. 164 (2017) E3569–E3575. https://doi.org/10.1149/2.0581711jes.
[58] P. Barai, K. Higa, V. Srinivasan, Lithium dendrite growth mechanisms in polymer electrolytes and prevention strategies, Phys. Chem. Chem. Phys. 19 (2017) 20493–20505. https://doi.org/10.1039/C7CP03304D.
[59] J.-N. Chazalviel, Electrochemical aspects of the generation of ramified metallic electrodeposits, Phys. Rev. A. 42 (1990) 7355–7367. https://doi.org/10.1103/PhysRevA.42.7355.
[60] Barton J. L., Bockris J. O'm., Ubbelohde Alfred Rene Jean Paul, The electrolytic growth of dendrites from ionic solutions, Proceedings of the Royal Society of London. Series A. Mathematical and Physical Sciences. 268 (1962) 485–505. https://doi.org/10.1098/rspa.1962.0154.

32

678

33